Thin–Walled Structures 159 (2021) 107307

Contents lists available at ScienceDirect

Thin-Walled Structures

journal homepage: http://www.elsevier.com/locate/tws

The application of the Wittrick-Williams algorithm for free vibration analysis of cracked skeletal structures

Xutao Sun

The School of Engineering, The University of Waikato, New Zealand

ARTICLE INFO

Keywords:
The Wittrick-Williams algorithm
Cracked beams
Dynamic stiffness method
Timoshenko beam
Rotary inertia

ABSTRACT

In this study, the dynamic stiffness method is applied to a cracked beam that incorporates Rayleigh bar theory and Timoshenko beam theory, and the Wittrick-Williams algorithm is used to pinpoint natural frequencies. The influence of a crack on the two components of the Wittrick-Williams algorithm, namely, the number of negative leading diagonal terms in the upper triangular form of the global dynamic stiffness matrix at a trial frequency, and the sum of frequencies of each clamped-clamped element of the structure exceeded by the trial frequency, is explored. For the first component, the leading diagonal terms relevant to the additional degrees of freedom introduced by the crack should be considered. While for the second component, it is shown that a crack element itself does not contribute to the second component. The influence of a crack element on the second component only lies in that the crack alters the discretization thus more beam elements are involved. The same philosophy applies to the introduction of an affiliated mass or spring-mass system. To verify this statement, the free vibration of a cracked single-storey frame carrying a roving mass with rotary inertia is studied. The frequency results obtained using the dynamic stiffness method incorporating the Wittrick-Williams algorithm are compared with those exported from a finite element model in ANSYS. Some discussions about the results are made. The effects of roving translational inertia and roving rotary inertia are studied.

1. Introduction

Structural engineers may often run into two eigenvalue problems, namely, the calculation for critical loads when structures are subjected to static loading and the calculation for natural frequencies in structural vibration problems. Among various techniques, the Wittrick-Williams (W-W) algorithm is an efficient eigensolver that has been used by many researchers [1–6]. When it is used in linear eigenvalue problems, it involves almost the same amount of work as the common technique in which the matrix $\boldsymbol{K}$ is converted to its upper triangular form $\boldsymbol{K}^{\Delta}$ then $|\boldsymbol{K}|$ is the product of leading diagonal terms in $\boldsymbol{K}^{\Delta}$. The only difference is that instead of computing $|\boldsymbol{K}|$, the W-W algorithm calls for trial values and the number of eigenvalues below the trial value is evaluated by the number of negative terms on the leading diagonal of $\boldsymbol{K}^{\Delta}$. However, when the W-W algorithm is used in transcendental eigenvalue problems, its superiority to common techniques is fully exhibited. It searches for eigenvalues in such a way that there is no possibility of missing any one of them. An instance of such a transcendental eigenvalue problem is the calculation for natural frequencies using the dynamic stiffness method (DSM). The DSM is regarded as an accurate method because in this method the structure is deemed to be continuous and uniform, thus no additional hypothesis (e.g. the lumped-mass hypothesis in the finite element method (FEM) and the Rayleigh-Ritz method) is needed except for the one made to derive the governing equation of motion. In the past decades, the DSM has been applied to structural members such as beams, columns, plates, and shells. In these applications, as the force-displacement relationship is obtained by solving the governing equation of motion, transcendental functions are involved in the dynamic stiffness matrix. Thus a reliable eigensolver is required and the (W-W) algorithm stands out.

Apart from intact structural members, the DSM is also used in problems regarding cracked members to investigate the dynamic response of structures in the presence of a crack. Generally speaking, there are four types of crack models, namely, the equivalent reduced cross-section model [7], the local flexibility model [8], the continuous flexibility model [9], and the special finite element model [10]. Among these models, the local flexibility model is most compatible with the DSM because by inverting the local flexibility matrix, the stiffness matrix of a crack element can be obtained and it can be easily integrated into the overall dynamic stiffness matrix. For example, Banerjee and Guo [2], Su and Banerjee [3] apply the DSM to a cracked beam based on the

E-mail address: briansun2018@hotmail.com.

https://doi.org/10.1016/j.tws.2020.107307
Received 29 July 2020; Received in revised form 1 November 2020; Accepted 11 November 2020
Available online 4 December 2020

Nomenclature

A	cross-sectional area
B	width of beam cross-section, see Fig. 4
$\boldsymbol{C}$	flexibility matrix of the crack element, see Eq. (12)
c	crack depth, see Fig. 4
E	Young's modulus
G	the shear modulus
H	height of beam cross-section, see Fig. 4
I	the second moment of area of the beam cross-section
I_p	the polar second moment of area
J_e	rotary inertia of the roving mass, see Fig. 8
J_{beam}	rotary inertia of the beam member about O' axis, see Fig. 9
j	number of natural frequencies below the trial frequency ω^*, see Eq. (26)
j_0	the sum of frequencies of each clamped-clamped element of the structure exceeded by the trial frequency ω^*, see Eq. (25)
$\boldsymbol{K}(\omega)$	the frequency-dependent global dynamic stiffness matrix
$\boldsymbol{K}(\omega^*)$	global dynamic stiffness matrix at the trial frequency ω^*
$\boldsymbol{K}(\omega^*)^{\Delta}$	the upper triangular form of dynamic stiffness matrix $\boldsymbol{K}(\omega^*)$
$\boldsymbol{K}_{cracked}(\omega)$	dynamic stiffness matrix of the crack beam, see Eq. (24)
$\boldsymbol{K}_{intact}(\omega)$	dynamic stiffness matrix of the intact beam, see Eq. (33)
$\boldsymbol{K}_{release}(\omega)$	dynamic stiffness matrix relevant to the nodes of the crack element, see Eq. (29)
$\boldsymbol{k}$	the inversion of flexibility matrix $\boldsymbol{C}$, see Eq. (18)
k	the shape factor
$\boldsymbol{k}^c$	a 6×6 stiffness matrix at the crack location, see Eq. (18)
$\boldsymbol{k}^e_{ij}$	sub-matrices of the dynamic stiffness matrix of a beam element (e), where $i = 1, 2$; $j = 1, 2$, see Eq. (1)
$\boldsymbol{k}^c_{ij}$	sub-matrices of the 6×6 stiffness matrix at the crack location, where $i = 1, 2$; $j = 1, 2$, see Eq. (19)
L	the length of a beam member of the frame, see Fig. 9
L_{c_i}	the location of a crack in the frame, where $i = 1, 2, 3, \cdots$, see Fig. 8
L_e	length of a beam element (e), where $e = a, b, c, \cdots$
M_e	translational inertia of the roving mass, see Fig. 8
M_{beam}	mass of the beam member, see Fig. 9
m	mass per unit length of the beam
$\boldsymbol{p}_i$	load vector at node i, where $i = 1, 2, 3, 4$
$s\{\boldsymbol{K}(\omega^*)^{\Delta}\}$	sign count i.e. the number of negative leading diagonal terms in $\boldsymbol{K}(\omega^*)^{\Delta}$, see Eq. (26)
$\boldsymbol{\delta}_i$	displacement vector at node i, where $i = 1, 2, 3, 4$
ν	Poisson's ratio
ξ	non-dimensional crack depth, see Eq. (17)
τ	the ratio between the roving translational inertia M_e and mass of the beam member M_{beam}, see Eq. (34)
ϕ	the ratio between the roving rotary inertia J_e and rotary inertia of the beam member J_{beam}, see Eq. (35)
ω	circular frequency
ω^*	arbitrarily chosen trial frequency

Euler-Bernoulli beam theory and the Timoshenko beam theory, respectively, and the (W-W) algorithm is used to search for natural frequencies. However, it is not mentioned why the (W-W) algorithm can be used to a cracked beam. Also, the influence of the crack element on the two terms in the (W-W) algorithm (i.e. $s\{\boldsymbol{K}(\omega^*)^{\Delta}\}$ and j_0 as shown in Eq. (26)) was not explained. In 2013, Caddemi and Calio [11] applied the DSM to a multi-cracked beam. The flexural stiffness of the beam was modified to incorporate the effect of cracks by introducing Dirac's delta singularities, thus the dimension of the overall dynamic stiffness matrix remained unaltered as the number of cracks increased. To calculate frequencies using the (W-W) algorithm, a sub-structuring method in which the cracked member was considered as a sub-structure was proposed to obtain j_0. In 2014, Labib et al. [12] applied the DSM to a cracked Euler-Bernoulli beam. In the overall dynamic stiffness matrix, rows and columns corresponding to the additional degrees of freedom introduced by the crack were eliminated by using partial Gaussian elimination, hence the dimension of the overall dynamic stiffness matrix of the cracked beam remained the same as that of the intact beam. Although the dimension remained unchanged regardless of the number of cracks, the eliminated terms must be accounted for when calculating $s\{\boldsymbol{K}^{\Delta}\}$ in the (W-W) algorithm to ensure that no frequency was missing.

It can be seen that despite the (W-W) algorithm is successfully employed in the abovementioned literature, no explanation is given regarding how the introduction of a crack influences $s\{\boldsymbol{K}(\omega^*)^{\Delta}\}$ and j_0. This article intends to answer this question. Following the research of Su and Banerjee [3,13], this study also adopts the DSM but includes more details concerning the application of the (W-W) algorithm. For each intact beam element, the Rayleigh bar theory and Timoshenko beam theory are used when deriving the dynamic stiffness matrix. Although the axial vibration and lateral vibration are uncoupled, the inclusion of the effects of shear deformation, rotary inertia, and inertia of lateral motions when cross-sections extend and contract in their own planes leads to more accurate results than those when using the simple bar theory and Euler-Bernoulli beam theory. To investigate the influence of a crack and an affiliated mass on the application of the (W-W) algorithm (more specifically, on the computation of j_0), the free vibration of a cracked single-storey frame carrying a roving mass with rotary inertia is studied within the framework of the DSM approach. A similar problem used to be tackled using the DSM but the roots are extracted by chasing the sign change of the determinant [14], which apparently risks the possibility of missing certain roots. To avoid such inaccuracy, in this study the (W-W) algorithm is employed to pinpoint natural frequencies. The DSM frequency results are compared with those obtained using FEM. Some discussions about the results are made. The effects of roving translational inertia and roving rotary inertia are studied.

2. The dynamic stiffness matrix of a cracked beam

Considering a cracked free-free beam as shown in Fig. 1, to investigate its free vibration characteristics using the DSM, the cracked beam is discretized into three elements denoted by letters (a), (b), and (c), as shown in Fig. 2. Thus, the cracked beam is represented by two Timoshenko beam elements (a) and (b), connected by a crack element (c), having lengths L_a, L_b, and L_c, respectively. In addition to the element lettering, the node numbering of the cracked beam is also shown in Fig. 2. For the demonstration, the length of the crack element is assumed

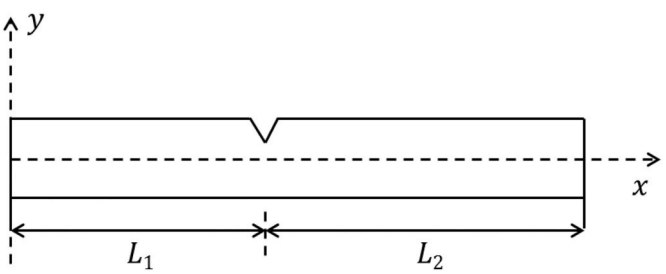

Fig. 1. A cracked free-free beam.

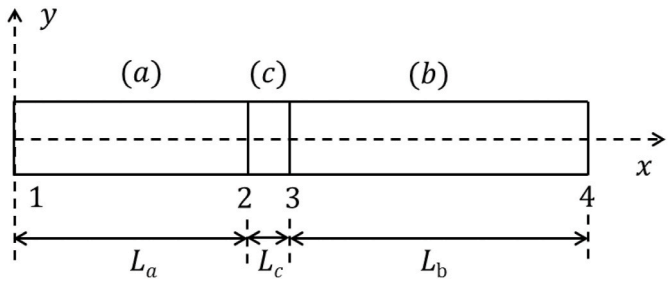

Fig. 2. Node numbering and element lettering of a cracked free-free beam.

to be L_c. It will be shown later that the stiffness matrix of the crack element (c) is derived from the local flexibility matrix at the cracked cross-section, which ends up being an equivalent spring stiffness matrix consisting of three mass-less springs (i.e. an axial spring, a lateral spring, and a rotational spring). Therefore, L_c actually represents the length of the cracked cross-section, which can be assumed as infinitesimal. And unlike a conventional elemental dynamic stiffness matrix which contains both mass and stiffness properties of the element as functions of structural parameters and the frequency [15], the stiffness matrix of the crack element (c) is independent of frequency as no mass-relevant term is included in it.

For a beam element incorporating the Rayleigh bar theory and Timoshenko beam theory, the dynamic stiffness matrix relating the amplitudes of forces (moments) and displacements (rotations) at nodes 1 and 2 can be found in the literature [13,16]. Referring to the nodal forces (moments) and displacements (rotations) shown for flexural motion in Fig. 3, the dynamic stiffness matrix relationship of a beam element (e) is given by

$$\begin{bmatrix} \boldsymbol{k}_{11}^e & \boldsymbol{k}_{12}^e \\ \boldsymbol{k}_{21}^e & \boldsymbol{k}_{22}^e \end{bmatrix} \begin{bmatrix} \boldsymbol{\delta}_1 \\ \boldsymbol{\delta}_2 \end{bmatrix} = \begin{bmatrix} \boldsymbol{p}_1 \\ \boldsymbol{p}_2 \end{bmatrix} \tag{1}$$

where

$$\boldsymbol{\delta}_1 = \{\delta_{x1}, \delta_{y1}, \theta_1\}^T; \boldsymbol{\delta}_2 = \{\delta_{x2}, \delta_{y2}, \theta_2\}^T; \tag{2}$$

$$\boldsymbol{p}_1 = \{f_{x1}, f_{y1}, m_1\}^T; \boldsymbol{p}_2 = \{f_{x2}, f_{y2}, m_2\}^T; \tag{3}$$

and T denotes a transpose. In Eq. (2), δ_{x1} and δ_{x2} are amplitudes of axial displacements, δ_{y1} and δ_{y2} are amplitudes of lateral displacements, θ_1 and θ_2 are amplitudes of rotations, at nodes 1 and 2, respectively. In Eq. (3), f_{x1} and f_{x2} are amplitudes of axial forces, f_{y1} and f_{y2} are amplitudes of shear forces, m_1 and m_2 are amplitudes of bending moments, at nodes 1 and 2, respectively.

–The dynamic stiffness elements of the sub-matrices $\boldsymbol{k}_{11}^e$ and $\boldsymbol{k}_{12}^e$ of Eq. (1) are frequency-dependent and are given by

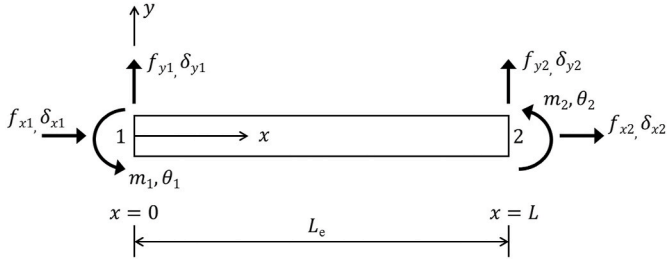

Fig. 3. Coordinate system and notation for forces (moments) and displacements (rotations) at nodes 1 and 2 of a Timoshenko beam.

$$\boldsymbol{k}_{11}^e = \begin{bmatrix} a_1^e & 0 & 0 \\ 0 & d_1^e & d_2^e \\ 0 & d_2^e & d_3^e \end{bmatrix} \text{ and } \boldsymbol{k}_{12}^e = \begin{bmatrix} a_2^e & 0 & 0 \\ 0 & d_4^e & d_5^e \\ 0 & -d_5^e & d_6^e \end{bmatrix} \tag{4}$$

where the terms are with regard to the beam parameters as follows

$$\left.\begin{aligned} a_1^e &= (EA/L_e)\gamma(1-\beta^2)\cot\gamma \\ d_1^e &= (EI/L_e^3)b^2\Gamma\left(C\overline{S}+\eta S\overline{C}\right)\Big/(\Lambda\Phi) \\ d_2^e &= (EI/L_e^2)Z\Gamma\left[(\Phi+\varepsilon\eta\Lambda)S\overline{S}-(\Lambda-\eta\Phi)\left(1-C\overline{C}\right)\right]\Big/(\Lambda+\eta\Phi) \\ d_3^e &= (EI/L_e)\Gamma\left(S\overline{C}-\varepsilon\eta C\overline{S}\right) \\ a_2^e &= -(EA/L_e)\gamma(1-\beta^2)cosec\gamma \\ d_4^e &= -(EI/L_e^3)b^2\Gamma\left(\overline{S}+\eta S\right)\Big/(\Lambda\Phi) \\ d_5^e &= (EI/L_e^2)Z\Gamma\left(\overline{C}-C\right) \\ d_6^e &= (EI/L_e)\Gamma\left(\varepsilon\eta\overline{S}-S\right) \end{aligned}\right\} \tag{5}$$

with

$$\left.\begin{aligned} Z &= \Phi - b^2s^2/\Phi \\ \eta &= Z/(\varepsilon\Lambda + b^2s^2/\Lambda) \\ \Gamma &= (\Lambda+\eta\Phi)\Big/\left[2\eta\left(1-C\overline{C}\right)+(1-\varepsilon\eta^2)S\overline{S}\right] \end{aligned}\right\} \tag{6}$$

$$\left.\begin{aligned} S &= sin\Phi \\ C &= cos\Phi \\ \Phi^2 &= \left[b^2(r^2+s^2)+b^2\sqrt{(r^2+s^2)^2+4(1-b^2r^2s^2)/b^2}\right]\Big/2 \end{aligned}\right\} \tag{7}$$

$$\left.\begin{aligned} &\overline{S} = sinh\Lambda; \overline{C} = cosh\Lambda \quad b^2r^2s^2 < 1(\varepsilon = 1) \\ &\overline{S} = sin\Lambda; \overline{C} = cos\Lambda \quad b^2r^2s^2 > 1(\varepsilon = -1) \\ &\varepsilon\Lambda^2 = \left[-b^2(r^2+s^2)\Big/2+b^2\sqrt{(r^2+s^2)^2+4(1-b^2r^2s^2)\Big/b^2}\right]\Big/2 \end{aligned}\right\} \tag{8}$$

In Eqs. (5)–(8)

$$\alpha^2 = \rho A\omega^2 L_e^2/(EA); \quad \beta^2 = \rho I_P\nu^2\omega^2/(EA); \quad \gamma^2 = \alpha^2/(1-\beta^2) \tag{9}$$

$$b^2 = \rho A\omega^2 L_e^4/(EI); \quad r^2 = I/(AL_e^2); \quad s^2 = EI/(kAGL_e^2) \tag{10}$$

where ω is the circular frequency, the subscript e refers to a specific beam element, and L_e, ρ, I_P, ν, k, G, EA and EI are the length of beam element, the density of the material, the polar second moment of area, the Poisson's ratio, the shape factor, the shear modulus, the axial rigidity, and the flexural rigidity, respectively.

$\boldsymbol{k}_{22}^e$ in Eq. (1) can be obtained from $\boldsymbol{k}_{11}^e$ by substituting $-d_2^e$ for d_2^e in Eq. (4), and $\boldsymbol{k}_{21}^e$ can be obtained by transposing $\boldsymbol{k}_{12}^e$. For a given trial frequency, it is thus possible to compute the dynamic stiffness terms of elements (a) and (b) in Fig. 2 by substituting the appropriate lengths L_a and L_b in Eqs. (5)–(10), respectively.

It should be noted that, from Eq. (10),

$$b^2r^2s^2 = \rho I\omega^2/kAG \tag{11}$$

For most practical problems, $b^2r^2s^2$ is less than one since the shear rigidity kAG is normally much bigger than $\rho I\omega^2$ unless ω is exceedingly large. Thus it is possible to omit the scenario when $b^2r^2s^2 > 1$ without ending up with erroneous results. However, for a fully clamped beam element with a short span, ω can reach large values within the first several modes of frequency, hence the circumstance when $b^2r^2s^2 > 1$ is no longer exceptional and should not be neglected. This is crucial and will be re-examined in Section 4.

The stiffness matrix for the crack element (c) in Fig. 2 can be obtained from the 3×3 flexibility matrix $\boldsymbol{C}$ given by [17–19]

$$\boldsymbol{C}=\begin{bmatrix} C_{11} & 0 & 0 \\ 0 & C_{22} & 0 \\ 0 & 0 & C_{33} \end{bmatrix} \tag{12}$$

The crack-induced local flexibility in skeletal structures can be evaluated by integrating the stress intensity factor. Zheng and Kessissoglou [20] have presented explicit expressions of C_{11}, C_{22} and C_{33} for beams with rectangular cross-section. For plane strain problems [2] and for a rectangular cross-section shown in Fig. 4, these expressions are taken from Zheng and Kessissoglou [20] and as follows

$$\left.\begin{array}{l} C_{11}=\left(1-\nu^2\right)\cdot F(1,1)/(EB) \\ C_{22}=\left(1-\nu^2\right)\cdot F(2,2)/(EB) \\ C_{33}=\left(1-\nu^2\right)\cdot F(3,3)/\left(EBH^2\right) \end{array}\right\} \tag{13}$$

where E is Young's modulus, B is the width of cross-section, H is the height of cross-section, and $F(1,1)$, $F(2,2)$ and $F(3,3)$ are non-dimensional functions given by [20]

$$\begin{aligned} F(1,1)=e^{1/(1-\xi)}\big(&-0.326584\times10^{-5}\xi+1.455190\xi^2-0.984690\xi^3 \\ &+4.895396\xi^4-6.501832\xi^5+12.792091\xi^6-26.723556\xi^7 \\ &+35.073593\xi^8-34.954632\xi^9+9.054062\xi^{10}\big) \end{aligned} \tag{14}$$

$$\begin{aligned} F(2,2)=e^{1/(1-\xi)}\big(&-0.326018\times10^{-6}\xi+1.454954\xi^2-1.455784\xi^3 \\ &-0.421981\xi^4-0.279522\xi^5+0.455399\xi^6-2.432830\xi^7 \\ &+5.427219\xi^8-6.643057\xi^9+4.466758\xi^{10}\big) \end{aligned} \tag{15}$$

$$\begin{aligned} F(3,3)=e^{1/(1-\xi)}\big(&-0.219628\times10^{-4}\xi+52.37903\xi^2-130.2483\xi^3 \\ &+308.442769\xi^4-602.445544\xi^5+939.044538\xi^6-1310.95029\xi^7 \\ &+1406.52368\xi^8-1067.4998\xi^9+391.536356\xi^{10}\big) \end{aligned} \tag{16}$$

with

$$\xi=c/H \quad (0\le\xi\le0.5) \tag{17}$$

is the non-dimensional crack depth, where c is the crack depth.

Once the flexibility matrix $\boldsymbol{C}$ of the crack element given by Eq. (12) is known, a 6×6 stiffness matrix $\boldsymbol{k}^c$ at the crack location can be constructed by using the inverse of $\boldsymbol{C}$ as follows

$$\boldsymbol{k}^c=\begin{bmatrix} \boldsymbol{C}^{-1} & -\boldsymbol{C}^{-1} \\ -\boldsymbol{C}^{-1} & \boldsymbol{C}^{-1} \end{bmatrix}=\begin{bmatrix} \boldsymbol{k} & -\boldsymbol{k} \\ -\boldsymbol{k} & \boldsymbol{k} \end{bmatrix} \tag{18}$$

where $\boldsymbol{k}$ is the inverse of $\boldsymbol{C}$.

Using the above stiffness matrix, the force-displacement relationship at the left and right ends of the crack element can now be formulated as

$$\begin{bmatrix} \boldsymbol{k}_{11}^c & \boldsymbol{k}_{12}^c \\ \boldsymbol{k}_{21}^c & \boldsymbol{k}_{22}^c \end{bmatrix}\begin{bmatrix} \boldsymbol{\delta}_L \\ \boldsymbol{\delta}_R \end{bmatrix}=\begin{bmatrix} \boldsymbol{k} & -\boldsymbol{k} \\ -\boldsymbol{k} & \boldsymbol{k} \end{bmatrix}\begin{bmatrix} \boldsymbol{\delta}_L \\ \boldsymbol{\delta}_R \end{bmatrix}=\begin{bmatrix} \boldsymbol{p}_L \\ \boldsymbol{p}_R \end{bmatrix} \tag{19}$$

where

$$\boldsymbol{\delta}_L=\left\{\delta_{xL},\delta_{yL},\theta_L\right\}^T;\boldsymbol{\delta}_R=\left\{\delta_{xR},\delta_{yR},\theta_R\right\}^T; \tag{20}$$

$$\boldsymbol{p}_L=\left\{f_{xL},f_{yL},m_L\right\}^T;\boldsymbol{p}_R=\left\{f_{xR},f_{yR},m_R\right\}^T; \tag{21}$$

It can be seen from Eq. (12) and Eqs. (18)–(21) that the stiffness matrix of the crack element (c) in Fig. 2 is equivalent to a spring stiffness matrix consisting of three mass-less springs i.e. an axial spring, a lateral spring, and a rotational spring, as shown in Fig. 5. The spring stiffness of these three springs are $1/C_{11}$, $1/C_{22}$, and $1/C_{33}$, respectively. Note that the stiffness matrix $\boldsymbol{k}^c$ corresponds to a crack element of infinitesimal length. Thus the length L_c appearing in Fig. 2 for the crack element is only for clarity and is discarded in Fig. 5.

Referring to Fig. 5 and using Eqs. (1)–(18), the force-displacement relationship of the cracked beam can be written as

$$\boldsymbol{K}_{cracked}(\boldsymbol{\omega})[\boldsymbol{\delta}_1,\boldsymbol{\delta}_2,\boldsymbol{\delta}_3,\boldsymbol{\delta}_4]^T=[\boldsymbol{p}_1,\boldsymbol{p}_2,\boldsymbol{p}_3,\boldsymbol{p}_4]^T \tag{22}$$

or

$$\boldsymbol{K}_{cracked}(\boldsymbol{\omega})\cdot\boldsymbol{D}=\boldsymbol{F} \tag{23}$$

where $\boldsymbol{K}_{cracked}(\boldsymbol{\omega})$ is the frequency-dependent dynamic stiffness matrix of the cracked beam, $\boldsymbol{D}$ is the displacement amplitude vector, and $\boldsymbol{F}$ is the force amplitude vector. $\boldsymbol{K}_{cracked}(\boldsymbol{\omega})$ can be formed in the same way as in the FEM by assembling the stiffness matrices of two Euler-Bernoulli beam elements (a) and (b) and one crack element (c) as shown in Fig. 5. $\boldsymbol{K}_{cracked}(\boldsymbol{\omega})$ can be symbolically expressed as follows

$$\begin{aligned} \boldsymbol{K}_{cracked}(\boldsymbol{\omega})&=\begin{bmatrix} \boldsymbol{k}_{11}^a & \boldsymbol{k}_{12}^a & 0 & 0 \\ \boldsymbol{k}_{21}^a & \boldsymbol{k}_{22}^a+\boldsymbol{k}_{11}^c & \boldsymbol{k}_{12}^c & 0 \\ 0 & \boldsymbol{k}_{21}^c & \boldsymbol{k}_{22}^c+\boldsymbol{k}_{11}^b & \boldsymbol{k}_{12}^b \\ 0 & 0 & \boldsymbol{k}_{21}^b & \boldsymbol{k}_{22}^b \end{bmatrix} \\ &=\begin{bmatrix} \boldsymbol{k}_{11}^a & \boldsymbol{k}_{12}^a & 0 & 0 \\ \boldsymbol{k}_{21}^a & \boldsymbol{k}_{22}^a+\boldsymbol{k} & -\boldsymbol{k} & 0 \\ 0 & -\boldsymbol{k} & \boldsymbol{k}+\boldsymbol{k}_{11}^b & \boldsymbol{k}_{12}^b \\ 0 & 0 & \boldsymbol{k}_{21}^b & \boldsymbol{k}_{22}^b \end{bmatrix} \end{aligned} \tag{24}$$

For undamped free vibration, Eq. (24) leads to an eigenvalue problem $\boldsymbol{K}_{cracked}(\boldsymbol{\omega})\cdot\boldsymbol{D}=0$, which will be addressed in the next section using the Wittrick-Williams (W-W) algorithm. Various boundary conditions of a cracked beam can be achieved by deleting the specific row and column in $\boldsymbol{K}_{cracked}(\boldsymbol{\omega})$ corresponding to the degree of freedom that is constrained. The mode shapes of a cracked beam can be calculated by discretizing the cracked beam and ensuring that the crack is located between two nodes of an element, then assuming one of the nodal displacements (rotations) to be 1 and determining the rest of the displacements (rotations) with

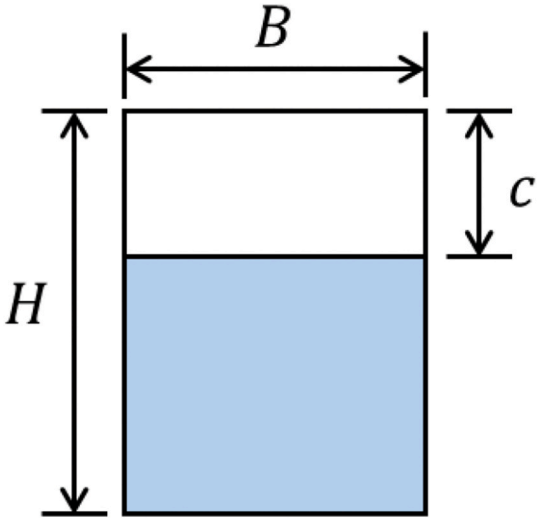

Fig. 4. Cross-sectional dimensions and crack depth of a cracked beam.

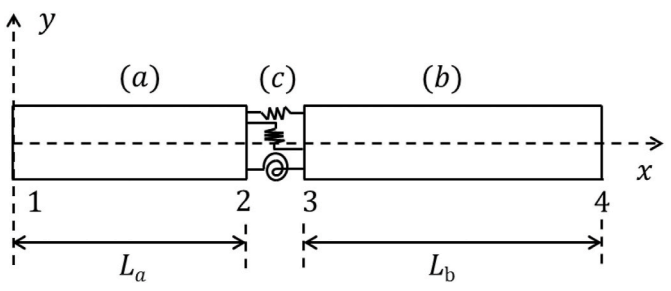

Fig. 5. The equivalent spring model of the crack element (c).

regard to the assumed one at a given frequency.

3. Application of the Wittrick-Williams (W-W) algorithm

The (W-W) algorithm [21,22] is regarded as an infallible method for solving eigenvalue problems. Thus it is also applicable for calculating natural frequencies and mode shapes of a structure using the DSM. As is demonstrated in the previous section, the overall dynamic stiffness matrix $\boldsymbol{K}(\omega)$ is formed by assembling elemental dynamic stiffness matrice(s). For the eigenvalue problem $\boldsymbol{K}(\omega)\cdot\boldsymbol{D} = 0$, two usual solution forms are well-researched: $|\boldsymbol{K}(\omega)| = 0; \boldsymbol{D} = 0$ with $|\boldsymbol{K}(\omega)| \to \infty$. In light of these two solution forms, two campaigns are implemented to search for frequencies. Firstly, assuming that none of the elements of $\boldsymbol{K}(\omega)$ become infinite at a trial frequency, which means the determinant of $\boldsymbol{K}(\omega)$ only changes its sign by crossing zero, the number of such zero points below the trial frequency is counted. Secondly, due to the existence of transcendental functions in Eqs. (5)–(10), assuming that one or more of the elements of $\boldsymbol{K}(\omega)$ becomes infinite at a trial frequency, which means, in this case, the determinant of $\boldsymbol{K}(\omega)$ changes its sign via infinity, the number of such poles (i.e. vertical asymptotes) below the trial frequency is counted. It is worth mentioning that a third solution form i.e. $|\boldsymbol{K}(\omega)| \neq 0$ with $\boldsymbol{D} \neq 0$ exists in some special circumstances when properties of structural members conform to certain relationships. It has been elucidated by Williams et al. [23] that this unusual form causes no problem when employing the (W-W) algorithm.

To be specific, the (W-W) algorithm can be applied in the following manner:

At an arbitrarily chosen trial frequency ω^*, the overall dynamic stiffness matrix $\boldsymbol{K}(\omega^*)$ is computed and Gaussian elimination (without row interchanges) is applied to $\boldsymbol{K}(\omega^*)$ to obtain the upper-triangulated form $\boldsymbol{K}(\omega^*)^{\Delta}$. The number of negative terms on the leading diagonal of $\boldsymbol{K}(\omega^*)^{\Delta}$ is counted. This is the so-called sign count $s\{\boldsymbol{K}(\omega^*)^{\Delta}\}$ which represents the number of zero points below the trial frequency ω^*.

The solution form ($\boldsymbol{D} = 0$ with $|\boldsymbol{K}(\omega)| \to \infty$) means that when all nodes of the structure are fully clamped, there still exist frequencies which would make $|\boldsymbol{K}(\omega)|$ approach infinity. This is because when using the DSM, the structure is regarded as a continuous system rather than an approximate lumped-mass system, which means an infinite number of degrees of freedom are accounted for and hence an infinite number of frequencies can be calculated. Thus one or more elements of the structure may still vibrate freely between nodes when all nodes are fully clamped. These frequencies are taken into account by the so-called j_0 count which is the sum of frequencies of each clamped-clamped element of the structure exceeded by the trial frequency ω^*, namely,

$$j_0 = \sum j_e \tag{25}$$

where j_e is the number of frequencies of each clamped-clamped element between $\omega = 0$ and $\omega = \omega^*$.

Thus

$$j = s\{\boldsymbol{K}(\omega^*)^{\Delta}\} + j_0 \tag{26}$$

where j is the number of natural frequencies below $\omega = \omega^*$. It can be seen from Eq. (26) that the (W-W) algorithm does not calculate frequency values directly. It is essentially an exquisite counting method through which any required frequency can be bracketed and converged on to any specified accuracy.

As the (W-W) algorithm is based on the Rayleigh's theorem [24] that can be verified for any linearly vibratory structure, it certainly can be applied to the cracked beam in Fig. 1. Before applying the (W-W) algorithm to complicated cracked skeletal structures, it is necessary to investigate how the introduction of a crack element affects $s\{\boldsymbol{K}_{cracked}(\omega^*)^{\Delta}\}$ and j_0. This question can be considered from two perspectives:

(i). As shown in Fig. 5, the crack element is equivalent to an element of infinitesimal length consisting of three mass-less springs, which means when both ends of this element are fully clamped, its frequency approaches infinity and hence is out of the frequency range we are investigating, or alternatively one may say there is no frequency for this clamped-clamped element. Thus in this case,

$$j_0 = j_a + j_b \tag{27}$$

where j_a and j_b is respectively the number of frequencies of the clamped-clamped element (a) and clamped-clamped element (b) exceeded by the trial frequency ω^*.

The $s\{\boldsymbol{K}_{cracked}(\omega^*)^{\Delta}\}$ of the cracked beam in Fig. 5 is composed of two parts as follows

$$s\{\boldsymbol{K}_{cracked}(\omega^*)^{\Delta}\} = s\{\boldsymbol{K}_{intact}(\omega^*)^{\Delta}\} + s\{\boldsymbol{K}_{release}(\omega^*)^{\Delta}\} \tag{28}$$

where $\boldsymbol{K}_{intact}(\omega^*)$ is the dynamic stiffness matrix of the intact beam at the trail frequency ω^*, and $\boldsymbol{K}_{release}(\omega^*)$ is a part of $\boldsymbol{K}_{cracked}(\omega^*)$. The terms in $\boldsymbol{K}_{release}(\omega)$ depend on the nodes of the crack element. As node 2 and node 3 are the nodes of the crack element, $\boldsymbol{K}_{release}(\omega)$ can be obtained from Eq. (24) by intercepting the overlap between the 2nd to the 3rd row and the 2nd to the 3rd column, giving

$$\boldsymbol{K}_{release}(\omega) = \begin{bmatrix} k^a_{22} + k & -k \\ -k & k^b_{11} + k \end{bmatrix} \tag{29}$$

Eq. (28) can be verified as follows:

For the free-free cracked beam in Fig. 5, referring to Eq. (24), its force-displacement dynamic stiffness relationship can be written as

$$\begin{bmatrix} k^a_{11} & k^a_{12} & 0 & 0 \\ k^a_{21} & k^a_{22} + k & -k & 0 \\ 0 & -k & k + k^b_{11} & k^b_{12} \\ 0 & 0 & k^b_{21} & k^b_{22} \end{bmatrix} \begin{bmatrix} \delta_1 \\ \delta_2 \\ \delta_3 \\ \delta_4 \end{bmatrix} = \begin{bmatrix} 0 \\ 0 \\ 0 \\ 0 \end{bmatrix} \tag{30}$$

From Eq. (30), δ_2 and δ_3 can be eliminated, leading to

$$\begin{bmatrix} \bar{k}_{11} & \bar{k}_{12} \\ \bar{k}_{21} & \bar{k}_{22} \end{bmatrix} \begin{bmatrix} \delta_1 \\ \delta_4 \end{bmatrix} = \begin{bmatrix} 0 \\ 0 \end{bmatrix} \tag{31}$$

where

$$\left.\begin{aligned} \bar{k}_{11} &= k^a_{21} - (k^a_{22} + k)(k^a_{12})^{-1} k^a_{11} \\ \bar{k}_{12} &= k(k^b_{21})^{-1} k^b_{22} \\ \bar{k}_{21} &= k(k^a_{12})^{-1} k^a_{11} \\ \bar{k}_{22} &= k^b_{12} - (k^b_{11} + k)(k^b_{21})^{-1} k^b_{22} \end{aligned}\right\} \tag{32}$$

As δ_2 and δ_3 are eliminated, Eq. (31) is the force-displacement dynamic stiffness relationship of an intact beam as shown in Fig. 6.

Therefore, the dynamic stiffness matrix of the intact beam can be written as

$$\boldsymbol{K}_{intact}(\omega) = \begin{bmatrix} \bar{k}_{11} & \bar{k}_{12} \\ \bar{k}_{21} & \bar{k}_{22} \end{bmatrix} \tag{33}$$

Applying the (W-W) algorithm to $\boldsymbol{K}_{intact}(\omega)$ would yield frequencies of a free-free intact beam. However, δ_2 and δ_3 are actually released due to the presence of the crack, hence the additional number of

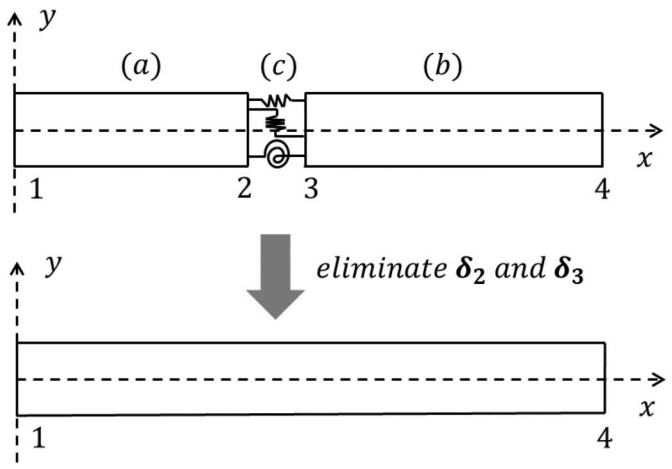

Fig. 6. Eliminate δ_2 and δ_3 in the free-free cracked beam.

frequencies resulting from the release of δ_2 and δ_3 should be accounted for. According to the proof of the (W-W) algorithm [22], for a structure with all of its $3N$ degrees of freedom fully clamped in the beginning, its degree of freedom is released one by one and f degrees of freedom are released, when the $(f+1)$th degree of freedom is released, the number of frequencies exceeded by a trial frequency ω^* would either increase by one or remain unaltered, which can be indicated by the sign of $k^{\Delta}_{(f+1)(f+1)}$ as $|\boldsymbol{K}_{(f+1)}(\boldsymbol{\omega}^*)| = |\boldsymbol{K}_f(\boldsymbol{\omega}^*)| \times k^{\Delta}_{(f+1)(f+1)}$. Likewise, for the cracked beam in Fig. 5, the release of δ_2 and δ_3 means the number of negative elements on the leading diagonal of $\boldsymbol{K}_{release}(\boldsymbol{\omega}^*)^{\Delta}$ should be counted. Therefore, Eq. (28) is verified.

It should be noted that Eq. (28) is designated to show how the introduction of a crack influences $s\{\boldsymbol{K}_{cracked}(\boldsymbol{\omega}^*)^{\Delta}\}$. When using the (W-W) algorithm, $s\{\boldsymbol{K}_{cracked}(\boldsymbol{\omega}^*)^{\Delta}\}$ of the cracked beam in Fig. 5 can be calculated directly using the $\boldsymbol{K}_{cracked}(\boldsymbol{\omega})$ in Eq. (24), and essentially the crack element can be treated as a special beam element that has zero length and has no direct contribution to j_0.

(ii). Also, the influence of a crack element on $s\{\boldsymbol{K}_{cracked}(\boldsymbol{\omega}^*)^{\Delta}\}$ and j_0 can be considered based on the implications of $s\{\boldsymbol{K}_{cracked}(\boldsymbol{\omega}^*)^{\Delta}\}$ and j_0. As aforementioned, j_0 represents the existence of the solution form ($\boldsymbol{D}=0$ with $|\boldsymbol{K}(\boldsymbol{\omega})|\to\infty$). Since there is no infinite term in the stiffness matrix of the crack element, a crack element itself does not contribute to j_0. Its influence on j_0 only lies in that it changes the discretization thus more beam elements are involved. An extension of this logic can be made to a multi-cracked frame structure in Fig. 7. Apart from multiple cracks, two mass and a spring-mass system are introduced as well. As the mass and spring-mass system do not bring new infinite terms to the overall dynamic stiffness matrix either, the change in j_0 only results from the new discretization as is shown by the dashed line in Fig. 7. Regarding $s\{\boldsymbol{K}_{cracked}(\boldsymbol{\omega}^*)^{\Delta}\}$, as long as the cracked structure is a linearly vibratory structure complying to Rayleigh's theorem [24], $s\{\boldsymbol{K}_{cracked}(\boldsymbol{\omega}^*)^{\Delta}\}$ can be computed in the usual way as stated in the (W-W) algorithm.

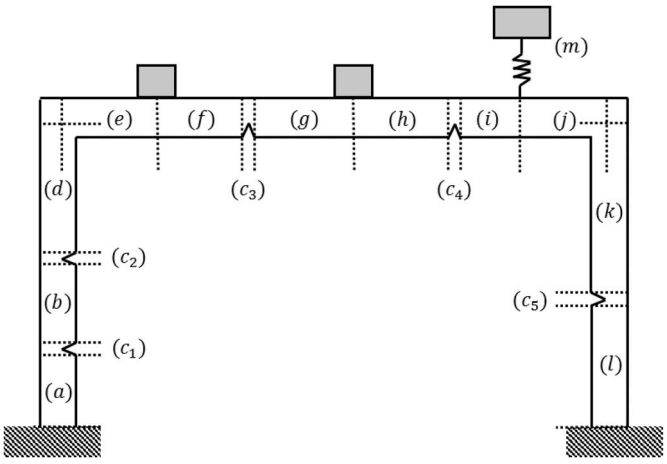

Fig. 7. A multi-cracked frame carrying mass and spring-mass system.

4. Numerical results and discussion

To verify the influence of a crack and an affiliated mass on the application of the (W-W) algorithm, in this section, a numerical example is given regarding a cracked frame carrying a roving mass with both translational and rotary inertias. The DSM is applied and the (W-W) algorithm is implemented to search for natural frequencies. The exact frequency results obtained using the DSM are compared with those computed using the FEM. In the FE modeling, cracks are simulated by cuts normal to the longitudinal axis of the structural member with a controlled depth. The width of the crack is carefully defined to ensure that both sides of the crack do not make contact for the first six modes of the vibration of the frame, thus avoiding the non-linear effects caused by crack closure which is out of the scope of this study.

4.1. Parameters of a cracked frame carrying a roving mass with rotary inertia

The free vibration of a cracked single-storey frame with both ends clamped carrying a roving mass is studied. A similar problem used to be solved by using the Matlab function *fzero*$(\cdot)$ [14], but here the first six natural frequencies are searched for using the (W-W) algorithm. Thus it can be ascertained that no frequency is missed. The mass roves on the middle member of the frame as shown in Fig. 8. Whenever the mass locates on a new position, frequencies of the frame are computed. Therefore, the velocity of the mass is not considered in the computation. The geometry of a beam member in the frame is shown in Fig. 9. Two cracks are introduced with one crack locating in the left member and the other in the middle member. As shown in Fig. 8, the crack depth c_1 in the left member is $0.004m$ (i.e. 20% of the beam height H) and the crack depth c_2 in the middle member is $0.006m$ (i.e. 30% of the beam height H).

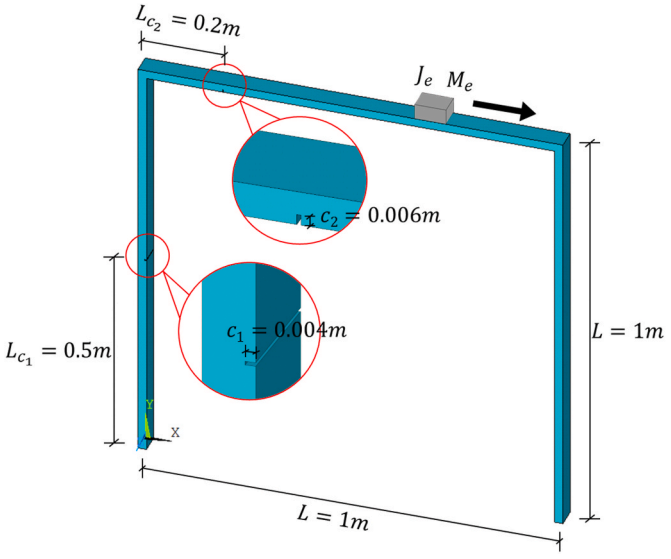

Fig. 8. The geometry of the cracked single-storey frame carrying a roving mass.

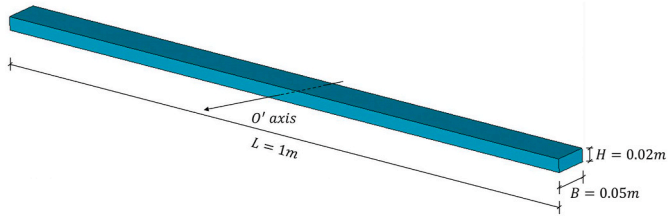

Fig. 9. The geometry of a beam member in the single-storey frame.

In Fig. 8, the translational inertia and rotary inertia of the roving mass are denoted as M_e and J_e, respectively. Ratios between inertias of the mass and beam member are denoted as follows

$$\tau = M_e / M_{beam} \tag{34}$$

$$\phi = J_e / J_{beam} \tag{35}$$

where M_{beam} and J_{beam} are specified in Table 1.

The dynamic stiffness matrices of a crack element and an intact beam member have been illuminated in Section 2. Subsequently, the global dynamic stiffness matrix can be constructed following the proper assembling order.

4.2. The global dynamic stiffness matrix

As shown in Fig. 10, there are two phases when the mass roves on the cracked frame. The cracked frame can be discretized into eight elements, i.e. six intact beam elements denoted as (a), (b), (d), (e), (f), (g), and two crack elements denoted as (c_1), (c_2). Two phases correspond to two different assembling sequences when constructing the global dynamic stiffness matrix, leading to two different forms of the global dynamic stiffness matrix.

The dynamic stiffness matrices of crack elements (c_1) and (c_2) can be integrated into the global dynamic stiffness matrix in the same manner as ordinary beam elements. The stiffness matrices of crack elements and beam elements in the local coordinate system are transformed into those in the global coordinate system according to the relation [25]:

$$\boldsymbol{K}_{global} = \boldsymbol{T}^T \boldsymbol{K}_{local} \boldsymbol{T} \tag{36}$$

where T is the transformation matrix given by

$$\boldsymbol{T} = \begin{bmatrix} \boldsymbol{t} & 0 \\ 0 & \boldsymbol{t} \end{bmatrix} \tag{37}$$

in which

$$\boldsymbol{t} = \begin{bmatrix} cos\theta & sin\theta & 0 \\ -sin\theta & cos\theta & 0 \\ 0 & 0 & 1 \end{bmatrix} \tag{38}$$

where θ is the relative angle between the local coordinate system and the global coordinate system, as shown in Fig. 11.

At each node that is shared by adjacent elements, the stiffness terms with regard to different degrees of freedom at the node are added together. Finally, the effect of concentrated inertias can be conveniently included in the matrix by adding $-M_e\omega^2$ to the diagonal term associated with mass lateral displacement and adding $-J_e\omega^2$ to the diagonal term associated with mass rotation. As the mass roves on the frame, the array of the length of beam elements is the principal variable. Thus the above process can be conveniently programmed using for loops in MATLAB. After the global dynamic stiffness matrix is formed, the (W-W) algorithm is applied to search for natural frequencies, which is presented in the next subsection.

Table 1
Physical parameters of the beam member.

beam density ρ	Young's modulus E	shear modulus G	Poisson's ratio ν	mass of the beam M_{beam}	rotary inertia of the beam about O' axis J_{beam}
7850 kg/m^3	200 GPa	76.9231GPa	0.3	7.85 kg	0.6544 kg·m^2

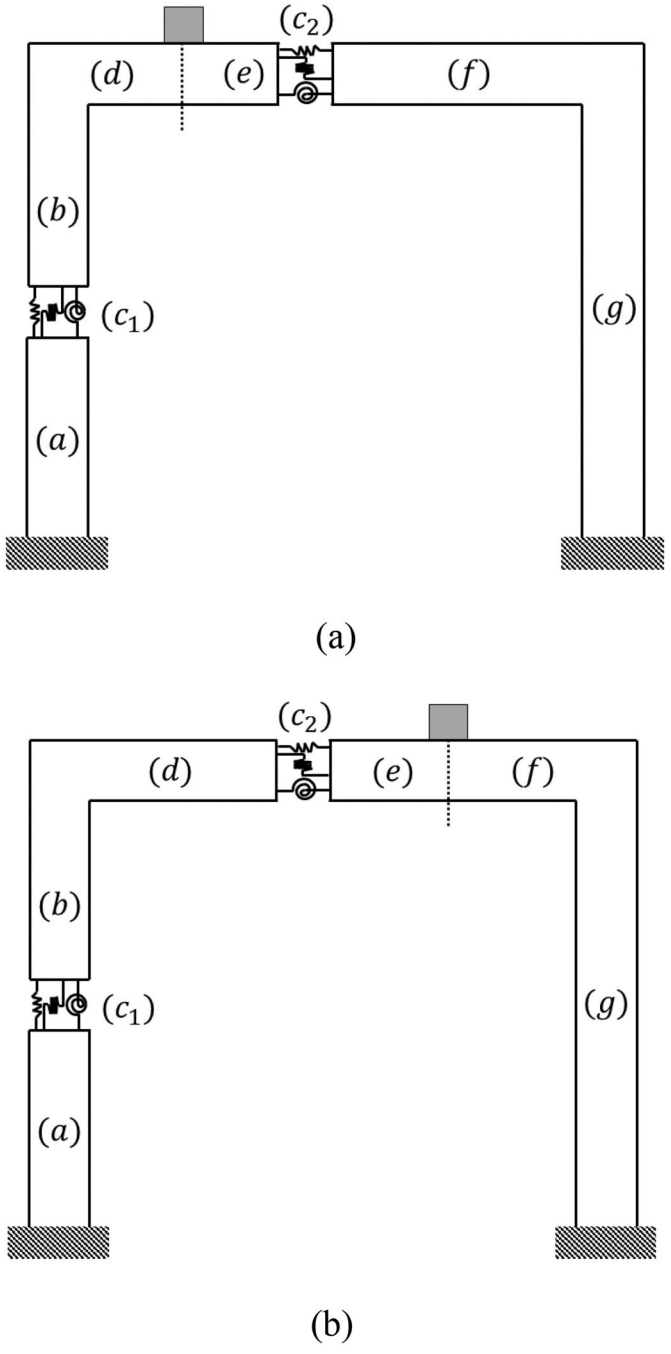

Fig. 10. The mass roves on the cracked frame: (a) on the left segment of the middle beam member, (b) on the right segment of the middle beam member.

4.3. Application of the Wittrick-Williams algorithm

According to Eqs. (25) and (26), the implementation of the (W-W) algorithm leads to

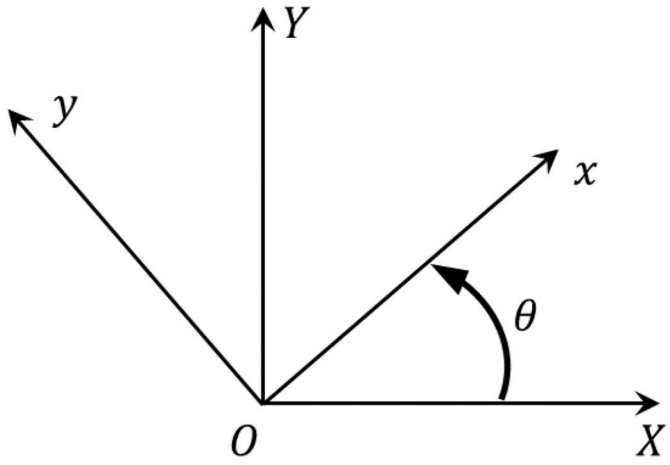

Fig. 11. The relative alignment of local (*Oxy*) and global (*OXY*) coordinate systems.

$$\begin{aligned} j &= s\{\boldsymbol{K}_{global}(\omega^*)^{\Delta}\} + j_0 \\ &= s\{\boldsymbol{K}_{global}(\omega^*)^{\Delta}\} + \sum j_e \end{aligned} \tag{39}$$

The determination of $s\{\boldsymbol{K}_{global}(\omega^*)^{\Delta}\}$ is relatively easy. However, for a cracked frame carrying a roving auxiliary system, j_0 should be calculated judiciously. As previously mentioned, the occurrence of a crack element and the inclusion of an affiliated mass influence j_0 only through the ensuing alteration in the discretization of the frame. Also, it can be seen in the last subsection that when assembling the global dynamic stiffness matrix, the crack element can be treated as a special beam element that has zero length and has no direct contribution to j_0. Overall, both the crack element and roving mass do not directly affect the computation of j_0.

As stated earlier, for each beam element, j_e in Eq. (39) is the number of frequencies exceeded by ω^* when the beam boundaries are fully clamped. It can be noticed from Fig. 10 that when the step size of the roving motion of the mass is small, the length of beam elements locating between the mass and crack may be short. Thus it is possible that frequencies of these beam elements become excessively large when the beam boundaries are fully clamped. In this case, according to Eq. (11), $b^2r^2s^2$ may surpass one, which indicates the change in the expressions of terms in the dynamic stiffness matrices of these elements. Therefore, the once exceptional circumstance where $b^2r^2s^2 > 1$ is no longer unusual and should be duly noted when preparing the dynamic stiffness matrix of the beam element.

According to Eqs. (4) and (5), the dynamic stiffness matrix of a Rayleigh bar element can be written as follows

$$\boldsymbol{K}_{bar} = \begin{bmatrix} a_1^e & a_2^e \\ a_2^e & a_1^e \end{bmatrix} = (EA/L_e)\gamma(1-\beta^2)\begin{bmatrix} cot\gamma & -cosec\gamma \\ -cosec\gamma & cot\gamma \end{bmatrix} \tag{40}$$

As previously mentioned, j_e represents the solution form ($\boldsymbol{D} = 0$ with $|\boldsymbol{K}(\omega)| \to \infty$). For a Rayleigh bar element, this solution form indicates that the bar is fully clamped and one or more terms in $\boldsymbol{K}_{bar}$ are infinite. From Eq. (40), it can be observed that this solution occurs when

$$\sin\gamma = 0 \text{ and } \gamma \neq 0 \tag{41}$$

The roots of Eq. (41) is $\gamma = i\pi$ $(i = 1, 2, 3, \ldots)$ and the number of natural frequencies of a clamped-clamped Rayleigh bar exceeded by a trial frequency ω^* is

$$j_R = floor(\gamma/\pi) \tag{42}$$

The determination of j_T, namely, the number of natural frequencies of a clamped-clamped Timoshenko beam below a trial frequency ω^*, is not as straightforward as that of j_R. Following the procedure illustrated in Refs. [13,16,26], j_T can be expressed as

$$j_T = j_c - \left\{2 - sg\left(d_3^e\right) - sg\left[d_3^e - \left(d_6^e\right)^2 / d_3^e\right]\right\}/2 \tag{43}$$

where $sg(\,)$ is either $+1$ or -1 depending on the sign of the quantity within the brackets. d_3^e and d_6^e are defined in Eq. (5) and j_c is given by

$$\left.\begin{aligned} j_c &= floor(\Phi/\pi) \quad (b^2r^2s^2 < 1) \\ j_c &= floor(\Phi/\pi) + floor(\Lambda/\pi + 1) \quad (b^2r^2s^2 \geq 1) \end{aligned}\right\} \tag{44}$$

where Φ and Λ are defined in Eqs. (7) and (8). Therefore, for a clamped-clamped beam element combining Rayleigh's bar theory and Timoshenko's beam theory, the number of frequencies exceeded by an arbitrarily chosen trial frequency ω^*, namely, j_e, is given by

$$j_e = j_R + j_T \tag{45}$$

Now the j_0 in Eq. (39) can be computed by doing summation of j_e over all the beam elements in the frame structure and the (W-W) algorithm can be implemented. The frequency results obtained using the DSM incorporating the (W-W) algorithm are compared with those exported from a FE model and are discussed in the next subsection.

4.4. Results verification and discussion

A two dimensional (2D) FE model of a cracked single-storey frame carrying a roving mass is constructed using ANSYS parametric design language. To effectively model the crack as well as to yield results that are close to the theoretical results, the 6-node triangular PLANE183 solid elements and 2-node BEAM188 elements are used to discretize the cracked frame (see Fig. 12). BEAM188 element is capable of modeling slender to moderately stubby/thick beams as the shear-deformation effects are included. Thus it is suitable to model the intact beam member and the segment of beam member that is far from the crack location. The crack is modeled as a slot, and discretization in the cracked region is refined. To ensure the compatibility of deformation, the degrees of freedom are coupled at the joints of BEAM188 and PLANE183 elements. Two MASS21 elements, locating on the upper surface and lower surface respectively, are employed to model the roving mass. The translational inertia in the lateral direction is included by setting the mass

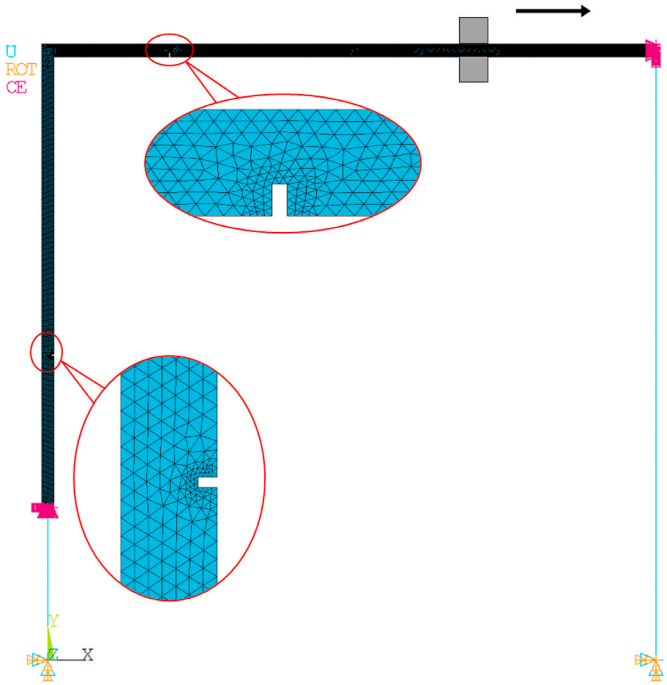

Fig. 12. Discretization of the FE model in ANSYS.

components in the Y direction. The rotary inertia is indirectly considered by setting the mass components in the X direction, thus the rotary inertia is accounted for by two translational inertias acting in the X direction with eccentricity being half of the beam height i.e. $H/2$. The mesh fineness of the FE model is determined after a number of convergence tests to substantially reduce the variance in results caused by discretization.

Firstly, the first six mode shapes and natural frequencies of the cracked frame without a roving mass are calculated using the DSM and are shown in Fig. 13. It can be seen that in the 1st and 3rd mode shape, the middle beam member undergoes both lateral bending and horizontal motion. Considering the fact that the roving mass is placed on the middle beam member and horizontal mass components are used to exert the rotary inertia in the FE model, the FEM results for the 1st and 3rd mode would be affected by the horizontal mass components and would deviate from the DSM results. Therefore, only the frequency results of the 2nd, 4th, 5th, and 6th mode are used for verification. When $\tau = 0.1$ and $\phi = 0.1.$, the curves for frequency versus mass location are shown in Fig. 14.

In Fig. 14, an excellent agreement between the DSM results and FEM results can be observed and despite minor discrepancies in frequency values, the trend of curves stays consistent. It demonstrates the correctness of DSM results and hence the successful application of the (W-W) algorithm. Abrupt frequency changes can be noticed in all frequency curves when the mass passes the crack at $x = 0.2m$. This phenomenon is consistent with the description in Ref. [14]. The crack brings about a rotation discontinuity of the beam cross-section, which leads to discontinuity in the inertial moment caused by affiliated mass, thus noticeable frequency change can be observed when the mass passes the rotation discontinuity i.e. the cracked cross-section. Since the inertial

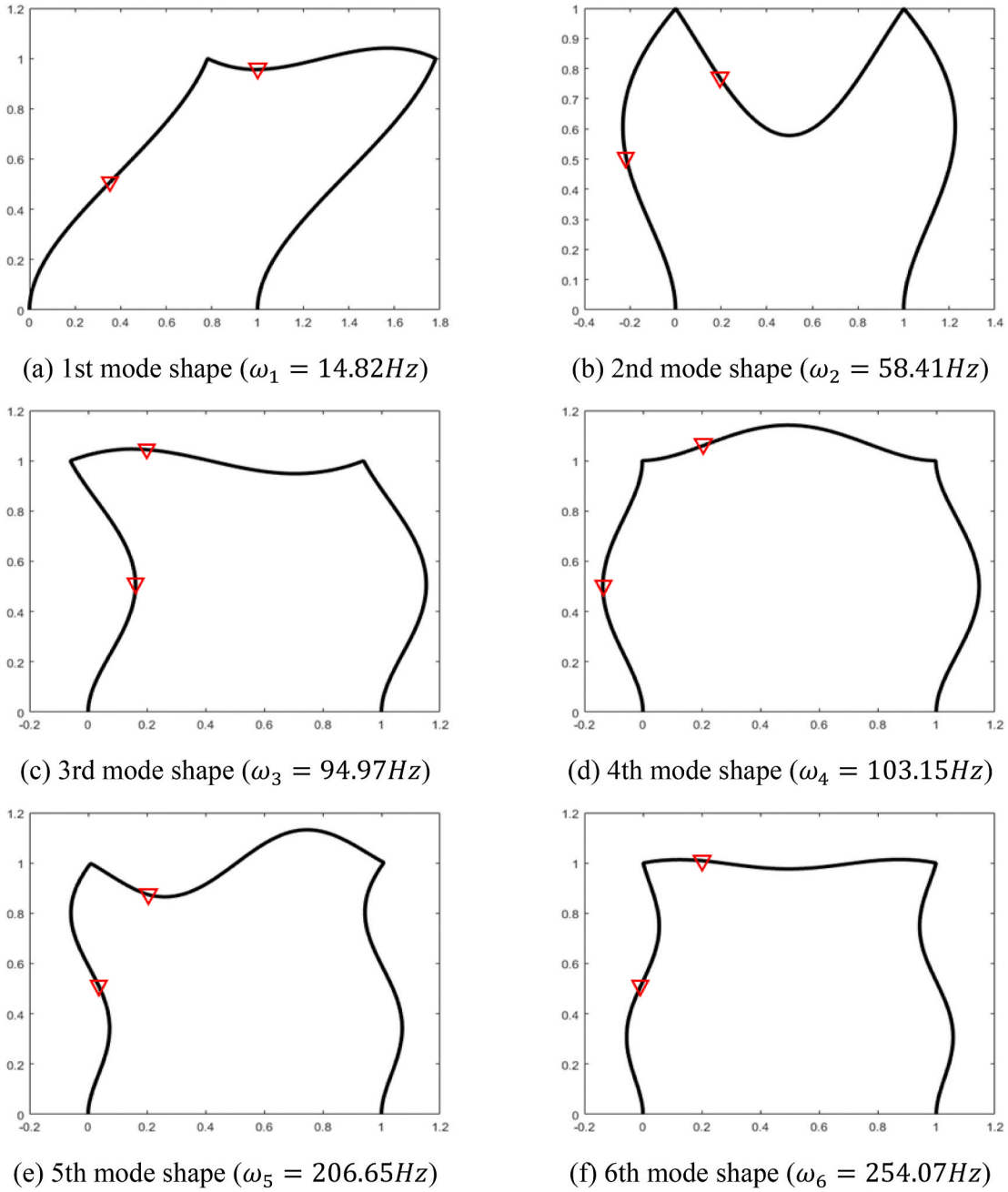

Fig. 13. DSM results of the first six modes of the cracked frame without a roving mass (red triangles represent the crack locations). (For interpretation of the references to colour in this figure legend, the reader is referred to the Web version of this article.)

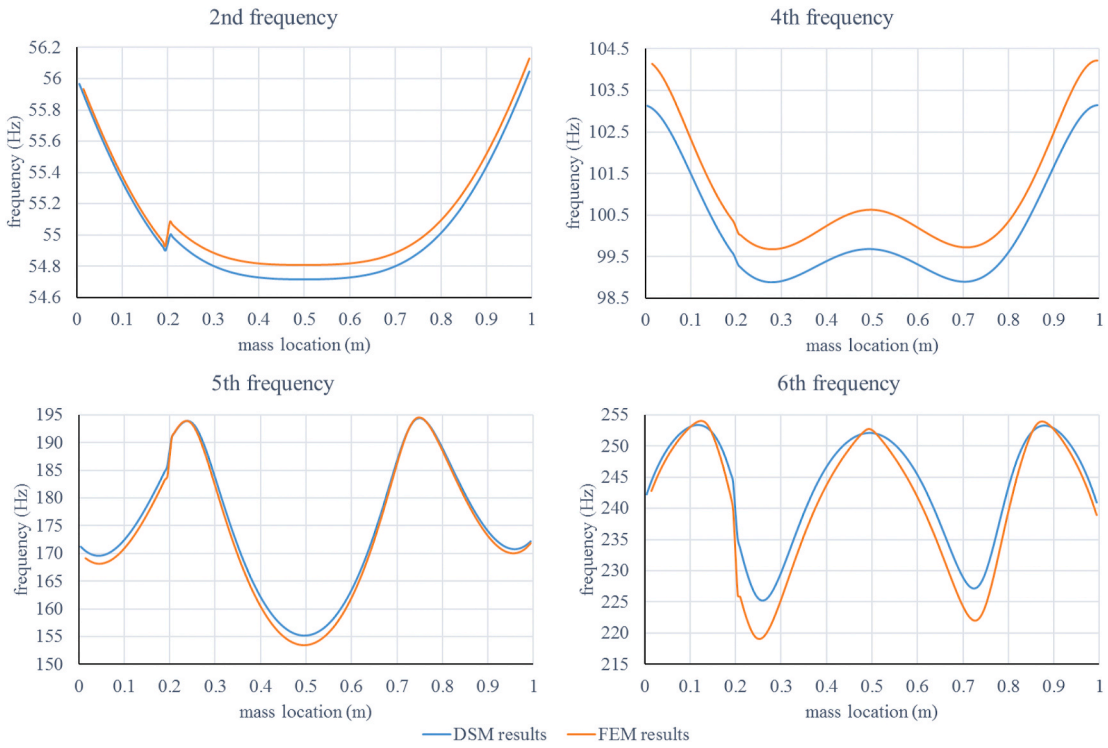

Fig. 14. The comparison between DSM results and FEM results ($\tau = 0.1$, $\phi = 0.1$).

moment is a product of rotary inertia, ω^2, and associated rotation of beam cross-section, the frequency change becomes more discernible as the mode of frequency rises. This can be displayed by doing subtraction between frequency results from two adjacent mass locations. For example, when the mass roves to a new position, the frequency result of the former position is subtracted from that of the current position, and the frequency shift is shown in Fig. 15. It can be noted that the magnitude of frequency shift when the mass passes the crack increases substantially as the mode of frequency rises.

In summary, the excellent agreement between the DSM results and FEM results demonstrates the success in two aspects: i) the correct assembling sequences of dynamic stiffness matrices as described in subsection 4.2; ii) the effective application of the (W-W) algorithm. It hence strengthens the previous statement that neither a crack element nor an affiliated mass has a direct contribution to j_0. In fact, their influence on j_0 only lies in that the discretization is altered thus more beam elements are involved (as shown in Figs. 7 and 10). In other words, j_0 in the (W-W) algorithm is independent of the crack severity and a roving

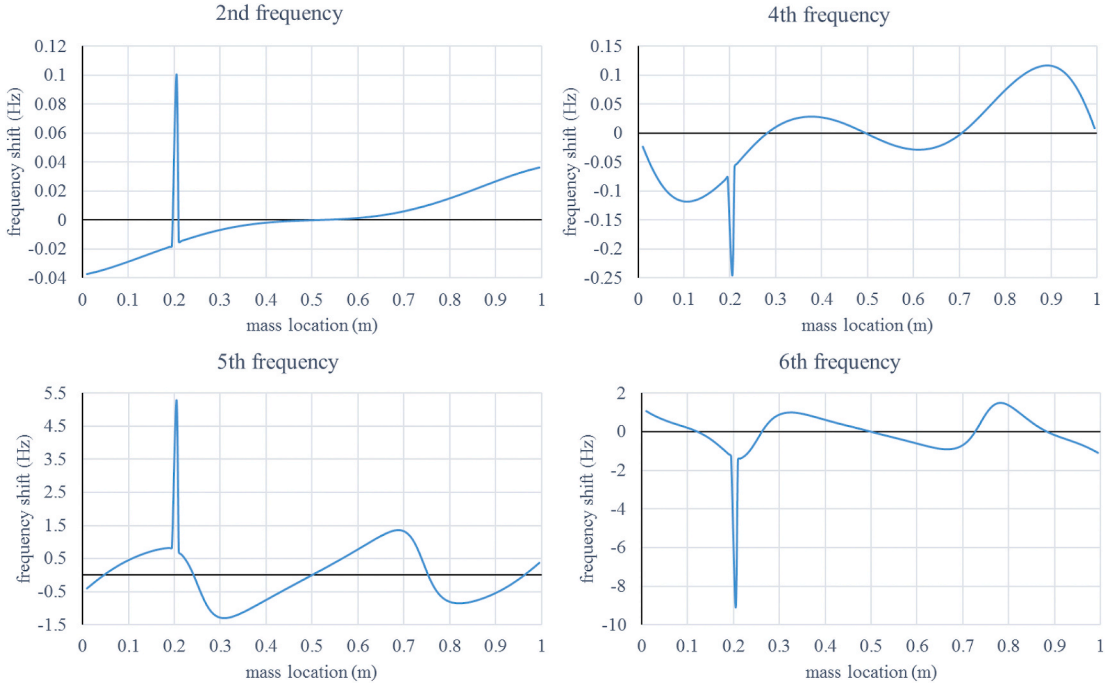

Fig. 15. The frequency shift calculated using the DSM results.

mass. Thus the effect of a roving mass or a roving constraint can be easily considered by modifying the global dynamic stiffness matrix. And j_0 can be calculated by considering all the intact beam elements. Compared with the solution in Ref. [14], the application of the (W-W) algorithm ensures that any particular natural frequency can be converged upon with certainty.

As the DSM results are verified, consequently, the effect of translational inertia and rotary inertia can be investigated using the DSM incorporating the (W-W) algorithm. This is discussed in the next subsection.

4.5. The effect of roving translational inertia and roving rotary inertia

When $\phi = 0.01$, different translational inertia values are tried and frequency results are shown in Fig. 16. Here we denote the structure in which the roving translational inertia is replaced by a roving lateral constraint as the lateral constrained structure (see Fig. 17). It can be observed that as the roving translational inertia increases the frequency decreases and converges to a specific value. For instance, in the graph of 2nd frequency, as the roving translational inertia grows, the frequency curve converges to the curve of 1st frequency of the lateral constrained structure (the green curve). The same phenomenon can be observed in graphs of 4th, 5th, and 6th frequency but with the green curve indicating the 3rd, 4th, and 5th frequency of the lateral constrained structure respectively. This phenomenon can be explained by the Rayleigh's theorem [24] based on which the (W-W) algorithm is formulated. It is stated in the theorem that for a structure with ω_r and ω_{r+1} ($r = 1, 2, 3, \ldots$) being its rth and $(r+1)$th natural frequency respectively, when one constraint is imposed on the structure, the rth natural frequency $\omega_r^{'}$ of the constrained structure satisfies the inequalities

$$\omega_r \le \omega_r^{'} \le \omega_{r+1} \tag{46}$$

From Eq. (46) it can be seen that $\omega_r^{'}$ is a lower bound of ω_{r+1}. This is exactly what can be observed in Fig. 16 where rth frequency of the lateral constrained structure is always higher than rth frequency of the original structure, and $(r+1)$th frequency of the original structure is always bounded from below by rth frequency of the lateral constrained structure.

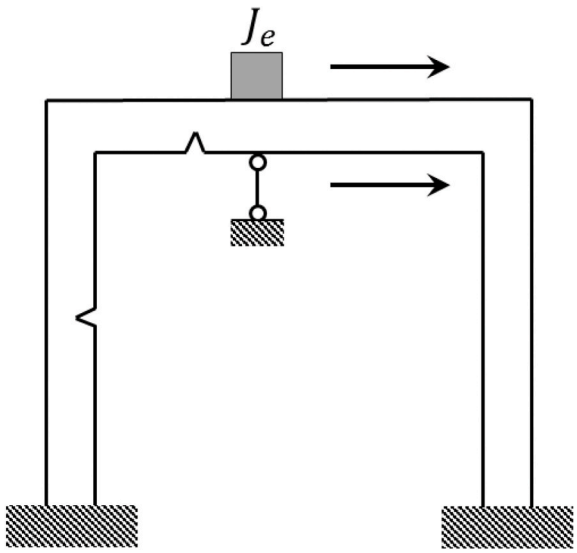

Fig. 17. The cracked frame carrying roving rotary inertia supported by a roving lateral constraint.

When $= 0.1$, various rotary inertia values are tried and frequency results are shown in Fig. 18. Here we denote the structure in which a roving rotational constraint is substituted for the roving rotary inertia as the rotational constrained structure (see Fig. 19). The phenomenon observed in Fig. 16 also appears in Fig. 18. Also, it can be noted in Fig. 18 that the abrupt frequency change when the roving rotary inertia passes the crack at $x = 0.2m$ can be discerned from curves of the 2nd frequency, while in Fig. 16 no visible abrupt frequency change can be found in all four frequency curves even when the roving translational inertia is very

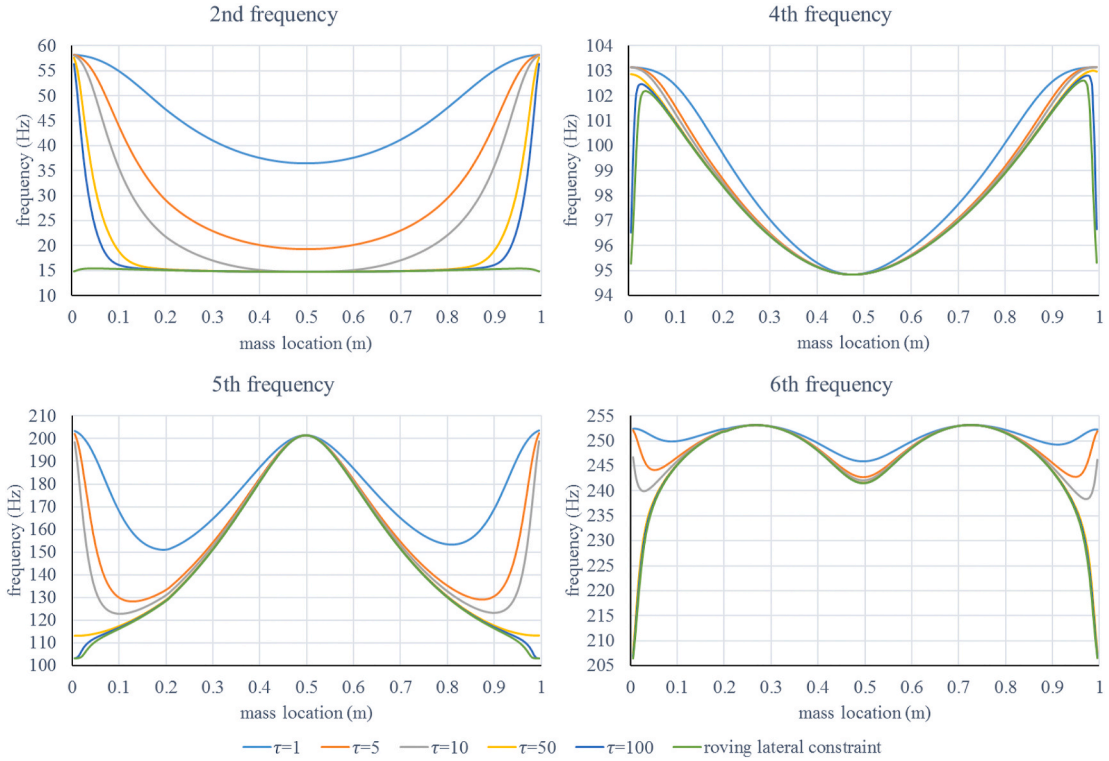

Fig. 16. The effect of various magnitudes of the roving translational inertia (when $\phi = 0.01$).

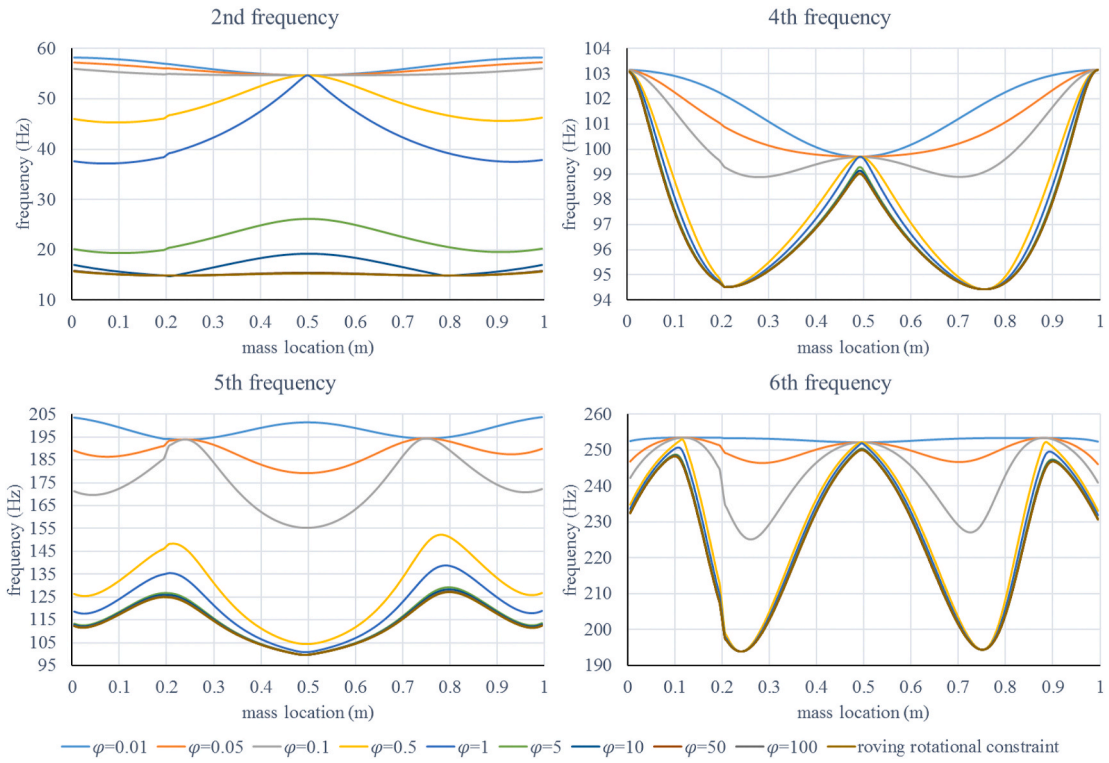

Fig. 18. The effect of various magnitudes of the roving rotary inertia (when $= 0.1$).

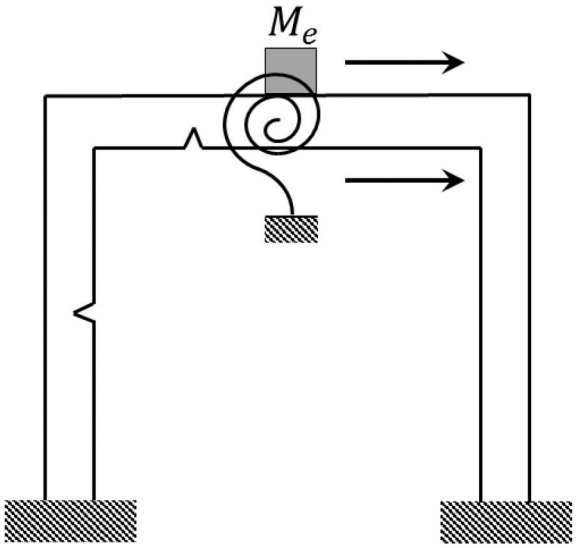

Fig. 19. The cracked frame carrying roving translational inertia supported by a roving rotational spring (the rotational spring stiffness approaches infinity).

large. This is as expected because even if the crack can be regarded as three springs (see Fig. 10), the rotational spring stiffness (i.e. $1/\ C_{33}$ in Eq. (18)) is much lower than the lateral spring stiffness (i.e. $1/\ C_{22}$ in Eq. (18)), thus the rotation discontinuity of the beam cross-section induced by the rotational spring is much severer than the lateral displacement discontinuity caused by the lateral spring. Hence the inertial moment caused by affiliated rotary inertia is much higher than the inertial force caused by affiliated translational inertia, leading to more discernible frequency changes.

5. Conclusions

This study applies the DSM to a cracked beam that incorporates Rayleigh bar theory and Timoshenko beam theory. The (W-W) algorithm is employed to solve the determinant of the global dynamic stiffness matrix. The question is answered regarding how the introduction of a crack influences $s\{\boldsymbol{K}(\boldsymbol{\omega}^*)^{\Delta}\}$ and j_0 in Eq. (26). For $s\{\boldsymbol{K}(\boldsymbol{\omega}^*)^{\Delta}\}$, the leading diagonal terms relevant to the additional degrees of freedom introduced by the crack should be taken into account. While for j_0, it is shown that a crack element itself does not contribute to j_0. Its influence on j_0 only lies in that it alters the discretization thus more beam elements are involved. Likewise, the same philosophy applies to the introduction of an affiliated mass or spring-mass system.

To verify the above explanation, within the framework of the DSM approach, the free vibration of a cracked single-storey frame carrying a roving mass with rotary inertia is studied. The procedure for integrating the global dynamic stiffness matrix is illustrated and the application of the (W-W) algorithm is elaborated. FEM frequency results are exported from a FE model to verify the DSM results. The excellent agreement between the DSM results and FEM results demonstrates the successful application of the (W-W) algorithm. It hence strengthens the statement that neither a crack element nor an affiliated mass has a direct contribution to j_0. Their influence on j_0 only lies in that the discretization is altered thus more beam elements are involved. The effect of a roving mass or a roving constraint can be easily considered by modifying the global dynamic stiffness matrix. The effects of roving translational inertia and roving rotary inertia are discussed. It is shown that as the affiliated roving inertias increase, the frequency curves converge to those when roving inertias are replaced by roving constraints. This is explained by Rayleigh's theorem [24] based on which the (W-W) algorithm is formulated.

In conclusion, it can be ascertained that j_0 in the (W-W) algorithm is independent of the crack severity and a roving mass. This characteristic makes it convenient to consider the effect of an auxiliary system, as long as the auxiliary system does not introduce new infinite terms to the global dynamic stiffness matrix.

Author statement

Xutao Sun: Conceptualization, Methodology, Software, Validation, Formal analysis, Visualization, Writing.

Funding

This research did not receive any specific grant from funding agencies in the public, commercial, or not-for-profit sectors.

Declaration of competing interest

The authors declare that they have no known competing financial interests or personal relationships that could have appeared to influence the work reported in this paper.

References

[1] J.R. Banerjee, et al., Free vibration of a three-layered sandwich beam using the dynamic stiffness method and experiment, Int. J. Solid Struct. 44 (22–23) (2007) 7543–7563.
[2] Banerjee, J.R. and S. Guo, On the dynamics of a cracked beam, in *50th AIAA/ASME/ASCE/AHS/ASC Structures, Structural Dynamics, and Materials Conference* 2009: Palm Springs, California.
[3] H. Su, J.R. Banerjee, Free vibration of a cracked Timoshenko beam using the dynamic stiffness method, in: 11th International Conference on Vibration Problems, Nova University of Lisbon, Lisbon, Portugal, 2013.
[4] A. Labib, D. Kennedy, C.A. Featherston, Crack localisation in frames using natural frequency degradations, Comput. Struct. 157 (2015) 51–59.
[5] S. Caddemi, I. Calio, F. Cannizzaro, The dynamic stiffness matrix (DSM) of axially loaded multi-cracked frames, Mech. Res. Commun. 84 (2017) 90–97.
[6] J. Banerjee, A. Ananthapuvirajah, Coupled axial-bending dynamic stiffness matrix for beam elements, Comput. Struct. 215 (2019) 1–9.
[7] T. Zheng, T. Ji, An approximate method for determining the static deflection and natural frequency of a cracked beam, J. Sound Vib. 331 (11) (2012) 2654–2670.
[8] J. Fernandez-Saez, L. Rubio, C. Navarro, Approximate calculation of the fundamental frequency for bending vibrations of cracked beams, J. Sound Vib. 225 (2) (1999) 345–352.
[9] T. Chondros, A. Dimarogonas, J. Yao, A continuous cracked beam vibration theory, J. Sound Vib. 215 (1) (1998) 17–34.
[10] A. Bouboulas, N. Anifantis, Formulation of cracked beam element for analysis of fractured skeletal structures, Eng. Struct. 30 (4) (2008) 894–901.
[11] S. Caddemi, I. Calio, The exact explicit dynamic stiffness matrix of multi-cracked Euler-Bernoulli beam and applications to damaged frame structures, J. Sound Vib. 332 (12) (2013) 3049–3063.
[12] A. Labib, D. Kennedy, C. Featherston, Free vibration analysis of beams and frames with multiple cracks for damage detection, J. Sound Vib. 333 (20) (2014) 4991–5003.
[13] J. Banerjee, A. Ananthapuvirajah, An exact dynamic stiffness matrix for a beam incorporating Rayleigh–Love and Timoshenko theories, Int. J. Mech. Sci. 150 (2019) 337–347.
[14] F. Cannizzaro, et al., On the use of a roving body with rotary inertia to locate cracks in beams, J. Sound Vib. 425 (2018) 275–300.
[15] J. Banerjee, Review of the dynamic stiffness method for free-vibration analysis of beams, Transport. Saf. Environ. 1 (2) (2019) 106–116.
[16] W. Howson, F. Williams, Natural frequencies of frames with axially loaded Timoshenko members, J. Sound Vib. 26 (4) (1973) 503–515.
[17] C. Papadopoulos, A. Dimarogonas, Coupling of bending and torsional vibration of a cracked Timoshenko shaft, Ing. Arch. 57 (4) (1987) 257–266.
[18] C. Papadopoulos, A. Dimarogonas, Coupled longitudinal and bending vibrations of a rotating shaft with an open crack, J. Sound Vib. 117 (1) (1987) 81–93.
[19] M. Kisa, J. Brandon, M. Topcu, Free vibration analysis of cracked beams by a combination of finite elements and component mode synthesis methods, Comput. Struct. 67 (4) (1998) 215–223.
[20] D. Zheng, N. Kessissoglou, Free vibration analysis of a cracked beam by finite element method, J. Sound Vib. 273 (3) (2004) 457–475.
[21] W.H. Wittrick, F. Williams, A general algorithm for computing natural frequencies of elastic structures, Q. J. Mech. Appl. Math. 24 (3) (1971) 263–284.
[22] F. Williams, W. Wittrick, An automatic computational procedure for calculating natural frequencies of skeletal structures, Int. J. Mech. Sci. 12 (9) (1970) 781–791.
[23] F. Williams, et al., Towards deep and simple understanding of the transcendental eigenproblem of structural vibrations, J. Sound Vib. 256 (4) (2002) 681–693.
[24] J.W. Strutt, The Theory of Sound. Cambridge Library Collection - Physical Sciences, vol. 2, Cambridge University Press, Cambridge, 2011.
[25] W. Howson, A compact method for computing the eigenvalues and eigenvectors of plane frames, Adv. Eng. Software 1 (4) (1978) 181–190, 1979.
[26] W. Howson, J. Banerjee, F. Williams, Concise equations and program for exact eigensolutions of plane frames including member shear, in: Engineering Software III, Springer, 1983, pp. 443–452.